Boundary-Layer Meteorol
DOI 10.1007/s10546-013-9805-2

ARTICLE

# Assimilating QuikSCAT Ocean Surface Winds with the Weather Research and Forecasting Model for Surface Wind-Field Simulation over the Chukchi/Beaufort Seas

**Xingang Fan · Jeremy R. Krieger · Jing Zhang · Xiangdong Zhang**

Received: 4 November 2011 / Accepted: 29 January 2013


**Abstract** To achieve a high-quality simulation of the surface wind field in the Chukchi/Beaufort Sea region, quick scatterometer (QuikSCAT) ocean surface winds were assimilated into the mesoscale Weather Research and Forecasting model by using its three-dimensional variational data assimilation system. The SeaWinds instrument on board the polar-orbiting QuikSCAT satellite is a specialized radar that measures ice-free ocean surface wind speed and direction at a horizontal resolution of 12.5 km. A total of eight assimilation case studies over two five-day periods, 1–5 October 2002 and 20–24 September 2004, were performed. The simulation results with and without the assimilation of QuikSCAT winds were then compared with QuikSCAT data available during the subsequent free-forecast period, coastal station observations, and North American Regional Reanalysis data. It was found that QuikSCAT winds are a potentially valuable resource for improving the simulation of ocean near-surface winds in the Chukchi/Beaufort Seas region. Specifically, the assimilation of QuikSCAT winds improved, (1) offshore surface winds as compared to unassimilated QuikSCAT winds, (2) sea-level pressure, planetary boundary-layer height, as well as surface heat fluxes, and (3) low-level wind fields and geopotential height. Verification against QuikSCAT data also demonstrated the temporal consistency and good quality of QuikSCAT observations.

X. Fan (✉)
Meteorology Program, Department of Geography and Geology, Western Kentucky University,
1906 College Heights Blvd., #31066, Bowling Green, KY 42101-1066, USA
e-mail: xingang.fan@wku.edu

J. R. Krieger
Arctic Region Supercomputing Center, University of Alaska Fairbanks, Fairbanks, AK, USA

J. Zhang
Departments of Physics and Energy and Environmental Systems, North Carolina A&T State University,
Greensboro, NC, USA

X. Zhang
International Arctic Research Center, University of Alaska Fairbanks, Fairbanks, AK, USA

Published online: 02 March 2013

**Keywords** Data assimilation · Numerical weather prediction · QuikSCAT ocean surface winds · Three-dimensional variational data assimilation · Weather Research and Forecasting model

## 1 Introduction

Ocean surface wind is a critical meteorological variable in the Chukchi Sea and Beaufort Seas region off Alaska's northern coast due to its role as the predominant driver of ocean currents, sea-ice motion, lead extent, and landfast ice breakout. As human activities such as near-shore oil and gas industrial development continue to increase along the Alaskan coast, oil spill and environmental assessments that demand high-resolution atmospheric and oceanic simulations and forecasts, including particularly those of surface wind, are required. The Chukchi and Beaufort Sea surface wind is primarily determined by prevailing local weather patterns that interact with prominent underlying geographical features encompassing complex surface conditions, including seasonal ice cover, open water, land, snow cover, and the Brooks Range to the south (Stegall and Zhang 2012). Chukchi and Beaufort Sea weather patterns are therefore highly variable both spatially, due to such complex mesoscale environmental factors as orographic forcing and land–snow–ocean–ice thermal contrasts, as well as temporally, due to larger-scale climatic changes (e.g., Kozo 1980, 1982; Walsh et al. 1996; Thompson and Wallace 1998; Zhang et al. 2004). Each of these presents a great challenge to the accurate modelling of surface winds in the area.

One major obstacle to the realistic simulation of the surface wind field in this region is the lack of a meaningful observational network, which hampers both factual analysis and accurate numerical modelling. In particular, the numerical weather prediction initial value problem relies on the accuracy of initial conditions, which ultimately derive from observations. Fortunately, more and more remotely-sensed data have become available in recent decades, providing a great amount of high spatial- and temporal-resolution data over the remote polar oceanic regions. Among these are several satellite-based near-surface ocean wind products, including those derived from Synthetic Aperture Radar (Pichel et al. 2005), the National Aeronautics and Space Administration (NASA) Scatterometer (NSCAT), the ERS-2 (Earth Resource Satellite, European Space Agency) Scatterometer (http://manati.orbit.nesdis.noaa.gov), the Special Sensor Microwave/Imager (SSM/I), the Advanced Scatterometer (ASCAT) on board MetOp satellites (http://oiswww.eumetsat.org/WEBOPS/eps-pg/ASCAT/ASCAT-PG-index.htm), and the SeaWinds Scatterometer on board the QuikSCAT satellite (http://podaac.jpl.nasa.gov/OceanWind/QuikSCAT). These data can be used to improve the simulation of the surface wind field via the application of data assimilation.

Data assimilation has been inextricably linked between these remotely-sensed data and numerical weather prediction. It is used to determine as accurately as possible the state of the atmosphere through an algorithm in which observations are merged with a dynamical numerical model of the flow. The objective of this merger is to identify an optimal estimate of the true atmospheric condition (e.g., Bengtsson et al. 1981; Daley 1991; Ide et al. 1997; Talagrand 1997; Kalnay 2003). Various techniques including optimal interpolation, one-, three-, and four-dimensional variational (1D-, 3D-, and 4D-VAR) methods, Kalman filter, extended Kalman filter, and ensemble Kalman filter have been developed and widely applied in the field of data assimilation.

Many studies have demonstrated a positive impact from the assimilation of satellite-derived winds. For example, Leidner et al. (2003) assimilated NSCAT data into the European Centre for Medium-Range Weather Forecasts (ECMWF) data assimilation system using a

4D-VAR approach to improve tropical cyclone forecasts; Isaksen and Janssen (2004) assimilated ERS winds into the ECMWF data assimilation system via both 3D- and 4D-VAR approaches to improve tropical cyclone and polar low forecasts; Chen et al. (2004) assimilated SSM/I winds and total column water vapour into the fifth-generation National Center for Atmospheric Research/Penn State Mesoscale Model (MM5) via 3D-VAR in a simulation of Hurricane Danny (1997); and Chen (2007) assimilated both SSM/I and QuikSCAT winds into MM5 via 3D-VAR to study the impact on the simulation of Hurricane Isidore (2002). From these studies, the variational approach has been shown to enable the consistent propagation of ingested information throughout the modelling domain.

Among these studies on the assimilation of satellite-derived surface winds, Chen (2007) compared the impacts of assimilating SSM/I and QuikSCAT wind data in a single-case study for Hurricane Isidore (2002). The assimilation of either of the wind products strengthened the cyclonic circulation in the resultant analysis, which produced a significant improvement in simulated storm intensity. Moreover, this study also demonstrated the superiority of QuikSCAT data to SSM/I winds due to the inclusion of wind direction in QuikSCAT.

The implementation of QuikSCAT surface wind data for the targeted high-latitude coastal Chukchi and Beaufort Sea region necessitates a more robust conclusion about its impact on the simulation of surface winds, as pointed out by Chen (2007). In addition, a new improvement to the QuikSCAT data has been included in the current study: the horizontal resolution has been increased from 25 to 12.5 km. This improvement is expected to have a greater impact on high-resolution surface wind-field simulations, a hypothesis that remains to be validated. In this study, the latest generation Weather Research and Forecasting model (WRF; Skamarock et al. 2005) and its 3D-VAR data assimilation system (WRFDA; Barker et al. 2004) are the vehicles used to ingest the QuikSCAT winds in the simulation of the Chukchi and Beaufort Sea surface wind field. Thus, this study also represents an opportunity to test the robustness of the WRFDA system in the high-latitude coastal regions through the assimilation of higher-resolution QuikSCAT data.

## 2 Modelling System Configuration and Data

The WRF model was established over the Chukchi and Beaufort Sea region with 10-km grid spacing and 43 vertical levels. The model domain (Fig. 1) encompassed the Alaskan North Slope and the Chukchi and Beaufort Seas; it is largely composed of ocean and a large portion of it is devoid of in situ measurements, including a lack of permanent buoys due to the annual encroachment of sea-ice. Initial and boundary conditions were provided by the 32-km resolution North American Regional Reanalysis (NARR) (Mesinger et al. 2006) and sea-ice data (0.5° resolution) were taken from the National Centers for Environmental Prediction (NCEP) Climate Data Assimilation System (Kistler et al. 2001). Model physical parametrizations included WRF Single-Moment 6-class microphysics (Hong et al. 2004), Kain-Fritsch cumulus (Kain and Fritsch 1990, 1993), Rapid Radiative Transfer Model longwave radiation (Mlawer et al. 1997), Dudhia (1989) simple shortwave radiation, the Noah land-surface model (Chen and Dudhia 2001), and the NCEP Eta planetary boundary-layer scheme (Janjic 1990, 1996, 2002).

In the WRFDA data assimilation system, both model background error covariances and observation error variances are required by the variational approach. A customized model background error was generated for the study domain (Fig. 1) from a series of 12- and 24-h WRF forecasts initialized every six hours throughout a 6-month period (May–October 2002) by using the so-called "NMC-method" (Parrish and Derber 1992).

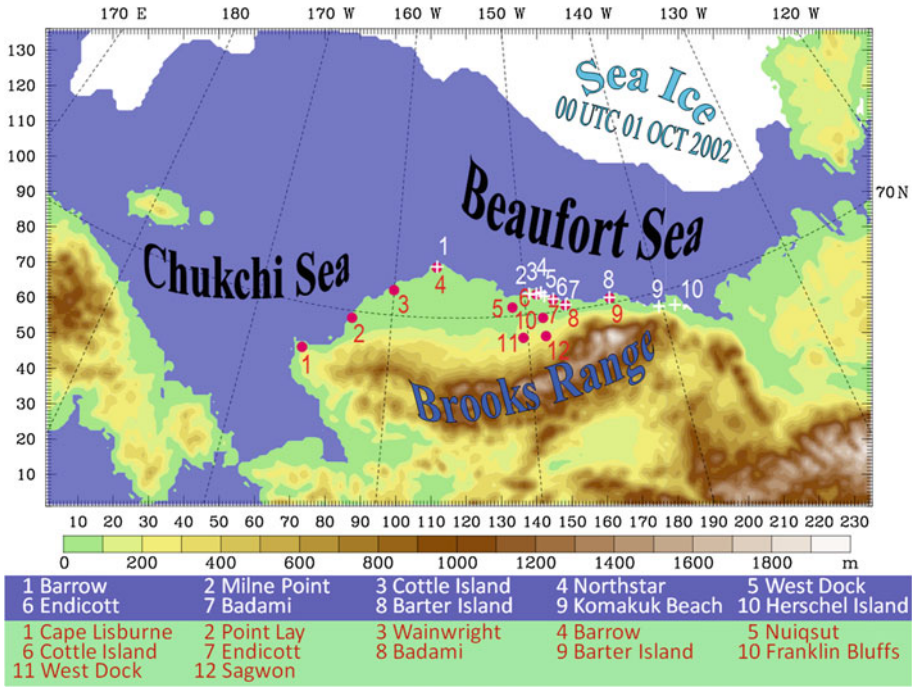


**Fig. 1** Modelling domain with land, sea, and ice distribution valid at 0000 UTC 1 October 2002. 12 stations (*red dots*) were used for model verification; 10 coastal and offshore stations (*white plus signs*) were used for QuikSCAT wind-error analysis

The observation error variances for the QuikSCAT ocean surface winds were obtained from an error analysis in which they were compared to near-shore station observations. As mentioned previously, there are no fixed buoys in the region of interest to use for such an analysis. Most of the existing coastal in situ observations are produced by different field campaigns. There are 10 near-shore or offshore stations (listed in Table 1 and indicated in Fig. 1 by the white plus signs) that have observed wind data during the study periods and are relatively close (within 30 km) to the QuikSCAT data offshore. These nearby coastal station observations (usually made on the hour) were compared with QuikSCAT data that were measured within 30 min of the station observation time. Table 1 lists the standard deviations of the differences in wind speed and direction between the QuikSCAT and station observations. The standard deviation of the difference in wind speed ranges from 1.2 to 2.4 m $s^{-1}$ with an average of 1.9 m $s^{-1}$; the standard deviation of the difference in wind direction ranges from 33 to 75° with an average of 46°.

Figure 2 shows scatter plots of the QuikSCAT versus station observations, including both wind speed and direction. In general, QuikSCAT wind speeds are larger than the corresponding station observations (Fig. 2a). The difference in locations between the QuikSCAT and station observations most likely explains the difference. The QuikSCAT winds were observed over the open ocean, where the surface friction is smaller than that over land, which undoubtedly leads to higher resultant surface wind speeds. In addition, stronger biases are seen for the lower wind speeds than for the high winds. Considering that there were very few QuikSCAT data points within 15 km of a coastal station, the actual observational errors should thus be less than what is shown in Table 1. As utilized in this study, QuikSCAT data

**Table 1** Standard deviation of differences between QuikSCAT surface winds and observations at 10 coastal stations

| Station | Speed (m $s^{-1}$) | Direction (°) |
|---|---|---|
| Badami | 1.72 | 44.48 |
| Barrow | 2.24 | 33.59 |
| Barter Island | 1.62 | 56.51 |
| Cottle Island | 1.40 | 39.36 |
| Endicott | 2.20 | 38.68 |
| Herschel Island | 2.44 | 53.97 |
| Komakuk Beach | 1.46 | 75.67 |
| Milne Point | 1.47 | 41.82 |
| Northstar | 1.16 | 51.21 |
| West Dock | 2.13 | 39.39 |
| Average | 1.86 | 46.53 |

within a distance of 5 km of a model grid point were used to verify model results. In the end, despite the distance between the QuikSCAT and station locations, the QuikSCAT wind speeds are reasonably close to the station observations, lending credibility to the accuracy of the product.

The wind directions are also generally similar between the two data sources (Fig. 2b), with some of the outliers clustered near the 180° difference on both sides of the diagonal line. The likely reason for this is that the QuikSCAT wind directions are not measured directly, but rather inferred from the orientation of the ocean waves. The instrument can thus only limit the direction to two possibilities that are perpendicular to the alignment of wave crests. To choose the appropriate direction, the retrieval algorithm incorporates wind data from a numerical model and selects the direction that is closest to the modelled direction (e.g., Long and Mendel 1990). The 180° error cluster is an implication of this limitation of the retrieval method. However, it is sufficient to observe that there are relatively few large discrepancies between the QuikSCAT and station wind directions. The discrepancies that do exist are also no doubt partially a result of the distance between the QuikSCAT and station locations, as well as the topographic impacts from the use of land-based coastal stations. An additional reason may be that the resolutions of the two data sources are different; QuikSCAT data represent average values over a 12.5 × 12.5 $km^2$ area, while station observations are made at a specific location.

These data comparisons and analyses give us confidence in assimilating QuikSCAT winds over the Chukchi and Beaufort Sea region. A wind-speed error variance of $(1.4\ m\ s^{-1})^2$ was reasonably representative for QuikSCAT wind speeds over the Beaufort Sea region in Chen (2007). Therefore, it was likewise adopted in this variational data assimilation study. Based on a similar consideration, the default wind direction error variance of $(20°)^2$ as set in the WRFDA system was used. Finally, the QuikSCAT data assimilated in this study have a resolution of 12.5 km, which is very close to the resolution of the model and therefore no data thinning was applied herein.

## 3 Study Cases and Modelling Experiment Design

Based on a screening of the ice-free area in the Chukchi and Beaufort Seas (where QuikSCAT data are available) and the prevailing wind field, two cases were selected in order to study the impact of assimilating QuikSCAT ocean surface winds on the modelling of the mesoscale

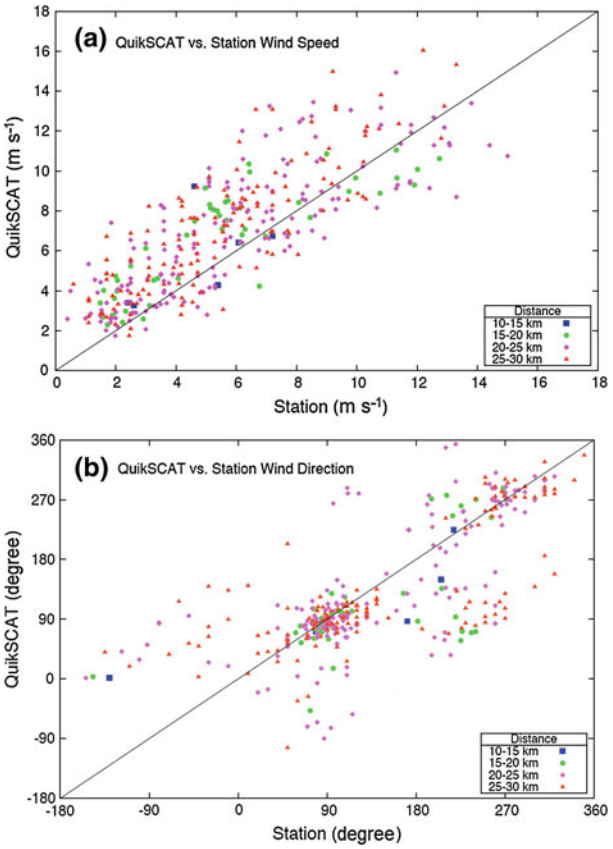


**Fig. 2** Scatter plots of QuikSCAT data versus station observations for: **a** wind speed (m $s^{-1}$) and **b** wind direction (°)

circulations of the Chukchi and Beaufort Seasregion: 1–5 October 2002 and 20–24 September 2004. Due to a relatively large ice-free area, there is a good availability of QuikSCAT winds over the region for these two periods. To facilitate their assimilation into the model, the QuikSCAT data were grouped into 1-h windows. Figure 3 illustrates the spatial and temporal availability of QuikSCAT data over a typical 1-day period from 0100 UTC 1 October to 0000 UTC 2 October 2002. The remaining days of the study periods have similar temporal distributions as those shown in Fig. 3. In addition, an analysis of the prevailing winds (not shown) revealed that these two cases experienced significant variability in the wind field, i.e., there were periods of both strong and weak winds, which makes these case studies more representative of the region's wind regime as a whole.

The modelling experiments were designed based on the temporal and spatial distributions of QuikSCAT winds over the study domain (Figs. 1, 3). The simulation starting and ending times were chosen so that the assimilation periods coincided with the times of day when the satellite passes were most frequent and thus sufficient data were available. Furthermore, the lengths of the simulations were chosen to ensure that QuikSCAT data were available at or near the end of assimilation period and were also available during the free-forecast period for model verification. Each of the 5-day periods was split into four 30-h periods,

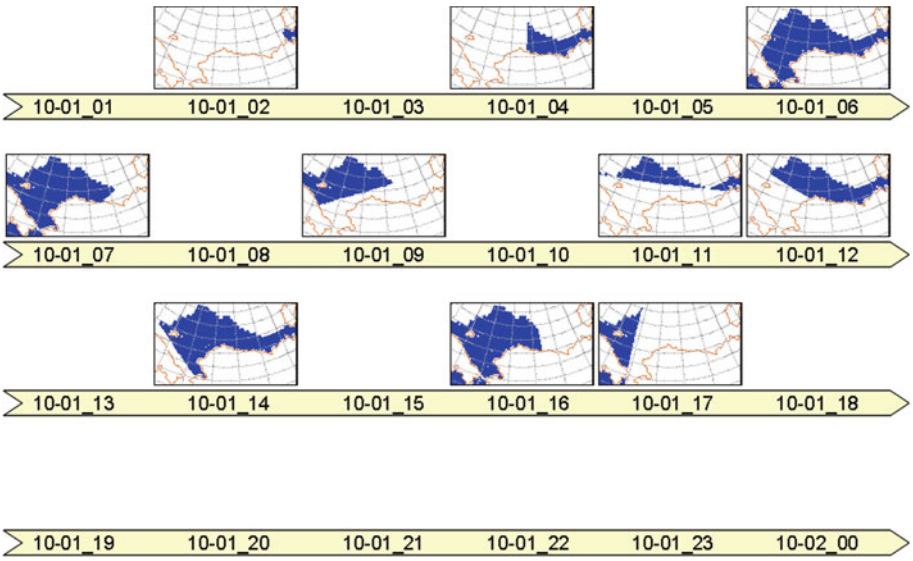


**Fig. 3** Typical one-day spatial coverage (*blue areas*) and temporal availability (*timelines*, in form of MM-DD_HH) of QuikSCAT ocean surface wind data from 0100 UTC 1 October to 0000 UTC 2 October 2002

beginning at 0000 UTC on each of the first four days. During each 30-h modelling period, QuikSCAT data were assimilated over the first six hours at 1-h intervals (for those hours that had data available). The QuikSCAT data were grouped into 1-h windows as described above and the model was integrated from the initial time up to an hour when QuikSCAT data were available, with the model output at this hour being used as the first-guess field for the WRFDA analysis. The available QuikSCAT observations within 30 min of this time were then assimilated. After a new 3D-VAR analysis field was generated, the simulation was continued from this new analysis with updated boundary conditions (also taken from the 3D-VAR analysis) until the next hour at which QuikSCAT data were available. The final assimilation time was at 0600 UTC in each assimilation experiment. A 24-h free-forecast period followed the 6-h assimilation period. Therefore, over the two 5-day periods there were a total of eight independent cases. Each of these cases was run twice, both with the assimilation of QuikSCAT winds (QSCAT run) and without (control run or CTRL hereafter). The QSCAT runs assimilated only QuikSCAT winds.

As noted in the previous section, the QuikSCAT retrieval algorithm utilizes a separate numerical model to identify the observed wind direction (Long and Mendel 1990), which constrains the data and ensures they are internally consistent. The prior analysis demonstrated that QuikSCAT data represent high-quality information for use in data assimilation. As the spatial resolution of the data closely matched that of the model, no further quality control procedures were deemed necessary for the purposes of this study.

## 4 Modelling Results

### 4.1 Impacts of QuikSCAT Data on 3D-VAR Analysis

It is necessary to first analyze the impact of QuikSCAT winds on 3D-VAR analysis to gain a better understanding of the overall impacts on surface wind simulations. Figure 4 shows the

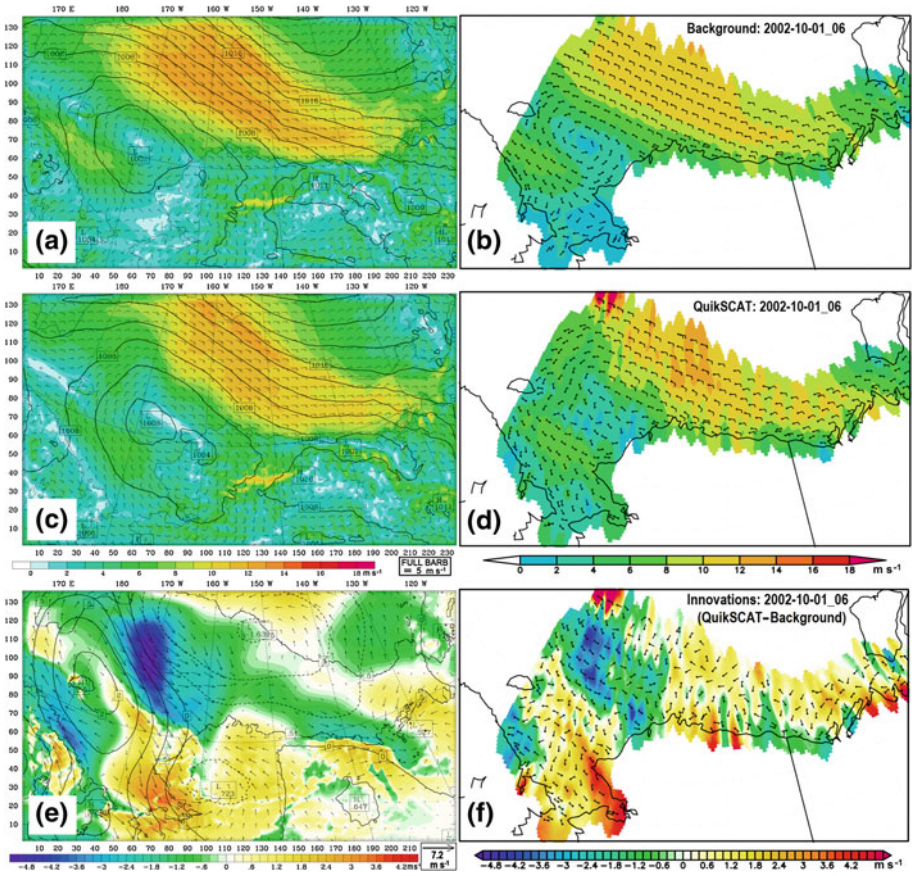


**Fig. 4** Sea-level pressure (hPa, *contour* in **a**, **c**, **e**), wind speed (m $s^{-1}$, *colour*), and wind barbs at the lowest model level from: **a** model forecast used as background (B); **b** background at QuikSCAT data points; **c** WRFDA analysis (A); **d** QuikSCAT data; **e** analysis increment (A–B); and **f** difference between QuikSCAT and background (innovations); all valid at 0600 UTC 1 October 2002. Wind data points have been thinned for illustration as wind barbs

3D-VAR analysis at 0600 UTC 1 October 2002 for the case starting at 0000 UTC, for which 0600 UTC is the end of the data assimilation period. The model simulation from the control run (CTRL) was used as the first-guess (background) field in the 3D-VAR analysis. Figure 4a shows example background fields of sea-level pressure and wind speed and direction at the lowest model level at 0600 UTC. There is a low-pressure system located over the Chukchi Sea and an area of high pressure along the north-eastern boundary of the domain, from which an area of strong south-easterly winds is maintained in the strong pressure-gradient zone over the Beaufort Sea. For ease in directly comparing the background winds to QuikSCAT, the background wind speed and direction were extracted at the locations of QuikSCAT data and are shown in Fig. 4b. Comparing these to the observed QuikSCAT wind speed and direction shown in Fig. 4d, the model simulation (Fig. 4b) captures the major wind patterns seen in the observations, particularly the strong south-easterly winds over the Beaufort Sea and the calm area over the Chukchi Sea. However, the simulated wind fields lack fine detail, while the QuikSCAT winds exhibit a more detailed structure within the area of strong winds,

despite the fact that the two fields possess similar resolutions. In addition, the simulated region of high wind speeds overextends to the west. The innovations (Fig. 4f), i.e., the difference field between observation and background, also called the O–B field, show that QuikSCAT observed higher wind speeds over the southern Chukchi Sea but lower speeds over the northern Chukchi Sea. Over the Beaufort Sea, the QuikSCAT wind speed is higher over the open water and generally lower along the Alaskan coast than in the model. This difference field, in conjunction with the model background, was applied via 3D-VAR to produce a new analysis field (Fig. 4c). The 3D-VAR analysis increment (Fig. 4e), i.e., the difference between the new analysis and background, reflects the features seen in the innovations field (Fig. 4f). However, the 3D-VAR analysis generated a slight reduction in wind speeds in the area north of the Alaskan coast between 159°W and 144°W in locations where QuikSCAT speeds were actually larger than in the model simulation. One possible reason for this discrepancy may be related to the model background error statistics that were calculated from an entire season's forecasts and therefore may not perfectly represent this particular case. The 3D-VAR analysis increment in the sea-level pressure field shows a decrease in the eastern half of the domain and an increase in the west, leading to an eastward shift of the weather systems present in the original model background (compare Fig. 4c and 4a). This change in sea-level pressure is consistent with that of the wind field, in which anticyclonic and cyclonic flows are seen in the difference field in the western and eastern halves of the domain, respectively (Fig. 4e).

## 4.2 Impacts of QuikSCAT Data on Forecasts

Analysis of the assimilation impacts and verification of the modelling results were done by comparing the model forecasts with the QuikSCAT data that were available during the free-forecast period, as well as with station observations. Note that during the free-forecast period, no data were assimilated. The average root-mean-square error, bias, and average absolute error for sea-level pressure and wind speed and direction were calculated. Statistics were averaged over each forecast hour over all cases, over every forecast hour for each individual case, as well as over all forecasts for each individual station in order to examine both the temporal and geographical distribution of the assimilation impacts. In addition, for purposes of comparison, the NARR re-analyses were also verified using the same criteria.

### *4.2.1 Verification Against QuikSCAT*

We first illustrate the verification analysis for the case of 1 October 2002. At 1200 UTC 1 October, six hours into the free-forecast period, there is a good availability of QuikSCAT data for use in verifying the model simulations (Fig. 5a). Figure 5b shows the forecasted differences in sea-level pressure, wind speed, and wind vectors between the QSCAT and CTRL experiments. The predominant features are similar to those of six hours before (ref. Fig. 4e), except for the eastward movement of the system and continued increase in sea-level pressure difference around the low-pressure system. Figure 5c, d show the differences in wind speed and direction between QuikSCAT (Fig. 5a) and the CTRL and QSCAT simulations, respectively. Compared to QuikSCAT, the CTRL experiment forecast higher wind speeds over the middle Beaufort and north Chukchi Seas, whilst the QSCAT experiment only forecast higher wind speeds over the north Chukchi Sea. The QSCAT experiment forecast lower wind speeds than did the CTRL experiment over most of the Beaufort Sea. Generally, the wind-speed error is within the range of $\pm 3$ m s$^{-1}$. In order to better investigate the surface-wind simulations from the two experiments over the entire domain, the absolute wind-speed error, defined as the absolute difference between modelled and QuikSCAT wind speeds,

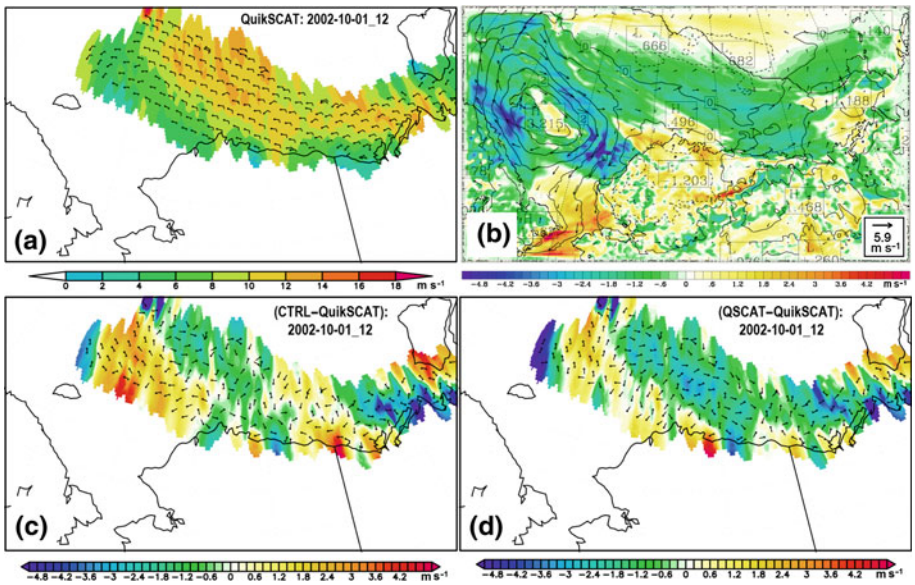


**Fig. 5** **a** QuikSCAT wind speed (m $s^{-1}$, *colour*) and wind barbs; **b** differences between the QSCAT and CTRL experiments for wind speed (m $s^{-1}$, *colour*) and wind vectors at the lowest model level and sea-level pressure (hPa, *contour*); **c** differences in wind speed (m $s^{-1}$, *colour*) and wind barbs at the lowest model level between the CTRL experiment and QuikSCAT; **d** same as (**c**) but between the QSCAT experiment and QuikSCAT. All fields are valid at 1200 UTC 1 October 2002, which is 6 h into the free-forecast period after data assimilation

was calculated. The result indicated that the absolute wind-speed error of the QSCAT run, averaged over the entire domain, was 0.7 m $s^{-1}$ smaller than that of the CTRL run. A similar analysis was conducted for wind direction, and the absolute wind-direction error was found to be generally less than 20° (not shown). Nevertheless, the absolute wind-direction error of the QSCAT run, averaged over the entire domain, was 1.1° smaller than that of the CTRL run. The superior results of the QSCAT wind speed and direction over the entire domain imply that assimilation of QuikSCAT data improved the 6-h wind forecast.

The above verification analysis was performed for all eight cases, using all QuikSCAT data available during the free-forecast periods. Since the QuikSCAT data are not available every hour, the statistical verification was instead performed on a three-hourly basis. In other words, the QuikSCAT data were grouped into 3-h windows centred on the model simulation hours of 6, 9, 12, 15, 18, 21, 24, 27, and 30. These hours correspond to the free-forecast hours of 0, 3, 6, 9, 12, 15, 18, 21, and 24 after the first 6-h data assimilation period. As shown in Fig. 6, the averaged root-mean-square error from all eight cases implies that the CTRL experiment has comparable errors in wind speed as the NARR reanalysis, though larger errors in wind direction. The wind speed and directions in the QSCAT experiment were improved for the first 12 h of the free-forecast period, suggesting that the assimilation of QuikSCAT winds had consistently positive impacts on the wind-field simulation over the open ocean, as verified against QuikSCAT data.

The assimilation of QuikSCAT data over the first six hours resulted in improved free forecasts in the QSCAT experiments, as demonstrated through verification with the subsequent 12-h unassimilated QuikSCAT data. Verification with station observations in the next subsection further supports this conclusion. In other words, assimilation of earlier QuikSCAT

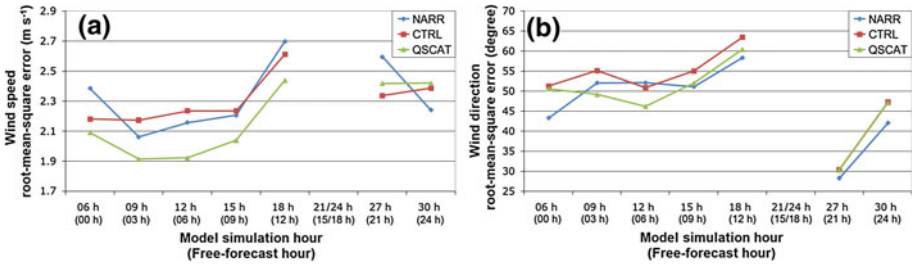


**Fig. 6** Root-mean-square error of modelled: **a** wind speed (m $s^{-1}$) and **b** wind direction (°) at the lowest model level for experiments CTRL and QSCAT, as well as for the NARR reanalysis, compared against QuikSCAT winds grouped into 3-h windows during free-forecast periods; averaged over all available QuikSCAT data and all eight cases

data produced simulations that are closer to later unassimilated QuikSCAT data; assimilation of QuikSCAT data also produced simulations that are closer to in situ observations. All of these imply the temporal consistency and good quality of QuikSCAT observations, and confirms that the data were also successfully assimilated into the model.

### *4.2.2 Verification Against Station Observations*

The usage of in situ observations is always desirable in model verification, particularly when remotely-sensed data are assimilated into the model. For this study, there were 12 coastal stations available for modelling verification as indicated by the red dots in Fig. 1. As was discussed in Sect. 2 (Fig. 2), there is generally good agreement between the station observations and QuikSCAT data, yet the large differences that do exist cannot be disregarded. Therefore, verification of model results against station observations is necessary to better demonstrate the broader impact of the assimilation of QuikSCAT winds. Figure 7 shows the averaged root-mean-square error and bias scores over the 12 stations and all eight cases for the modelled and NARR-analyzed surface (10-m height) wind speed and direction and sea-level pressure. In contrast to the verification against QuikSCAT winds (Sect. 4.2.1), where a positive impact was seen immediately in the wind-field forecasts (see Fig. 6), the verifications against the station data indicate a possible adjustment period during the first 3–6 h of the free-forecast, when the root-mean-square error of the wind speed in the QSCAT experiment is larger than that in the CTRL run. This adjustment period is seen primarily in the wind field (Fig. 7a–d), which is most likely due to the assimilation of the wind variable itself. From model simulation hour 18 (i.e., 12-h free-forecast time) and onward, however, the wind forecasts tend to be improved in the QSCAT experiment. Another possible factor in the worsening of the root-mean-square error in wind speed and direction at 1200 UTC could be the erroneously light winds in the NARR re-analysis, which provided initial and boundary conditions for the model.

As shown in Fig. 7e, f, the assimilation of QuikSCAT winds demonstrated a consistently positive impact on the sea-level pressure as verified against station observations. Both the root-mean-square error and bias for every forecast hour were reduced in the QSCAT experiment. Other variables, such as surface air temperature and humidity, experienced more varied results, without the consistent reduction in error observed for the wind fields, though an overall reduction in bias was seen (not shown).

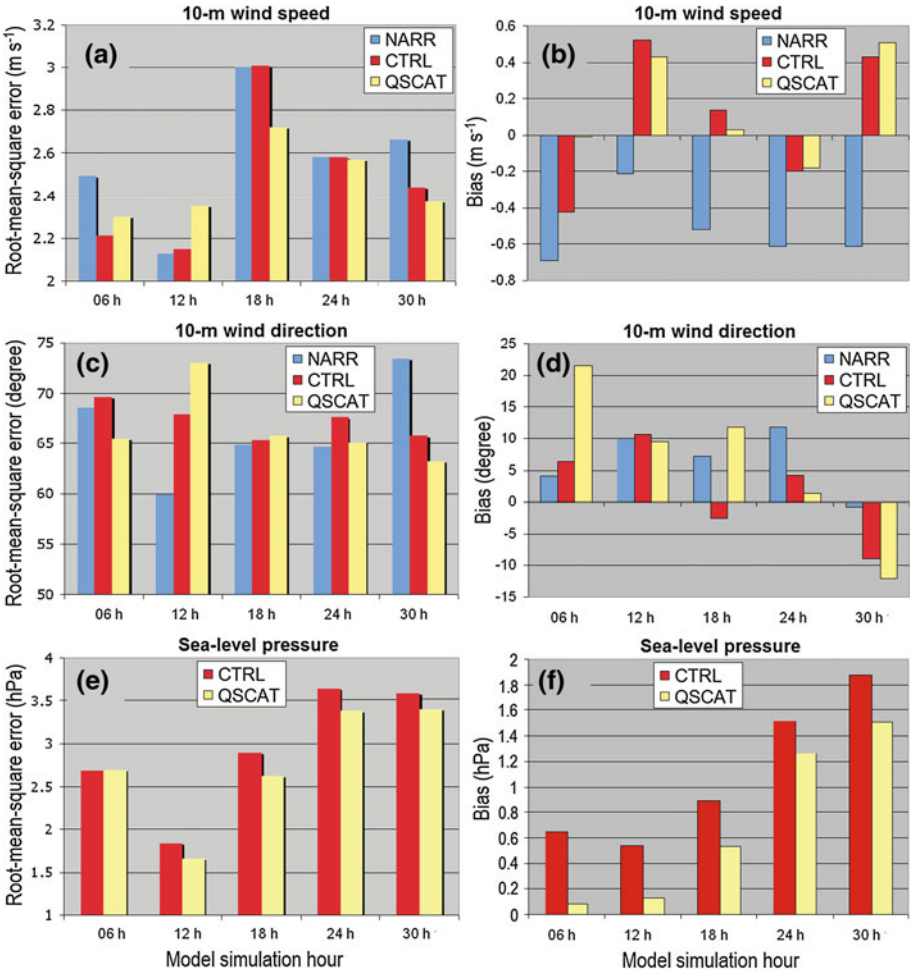


**Fig. 7** Root-mean-square error (*left column* **a**, **c**, **e**) and bias (*right column* **b**, **d**, **f**) of the 10-m wind speed (m $s^{-1}$, *top row* **a**, **b**), wind direction (°, *middle row* **c**, **d**), and sea-level pressure (hPa, *bottom row* **e**, **f**) from the experiments CTRL, QSCAT, and NARR re-analysis; calculated against station observations and averaged over 12 stations (see Fig. 1 *red dot* locations) and all eight cases, grouped by model simulation hour

### *4.2.3 Verification at Individual Stations*

Having seen the complexity of the impacts in the domain-averaged verification, we break the analysis down further to identify the impacts at different locations and areas through verification at each of the individual stations. This helps in investigating the characteristics of the impacts of assimilation along the complex coastal region. The model forecast errors were compared by plotting the differences in root-mean-square error between the QSCAT and CTRL experiments at each station for model simulation hour 18 (12 h into the free forecast), which occurs after the model adjustment period (Fig. 8). For the six stations that reported sea-level pressure data, the QSCAT run consistently improved the sea-level pressure forecast relative to the CTRL run. Wind direction in the QSCAT experiment was improved in the

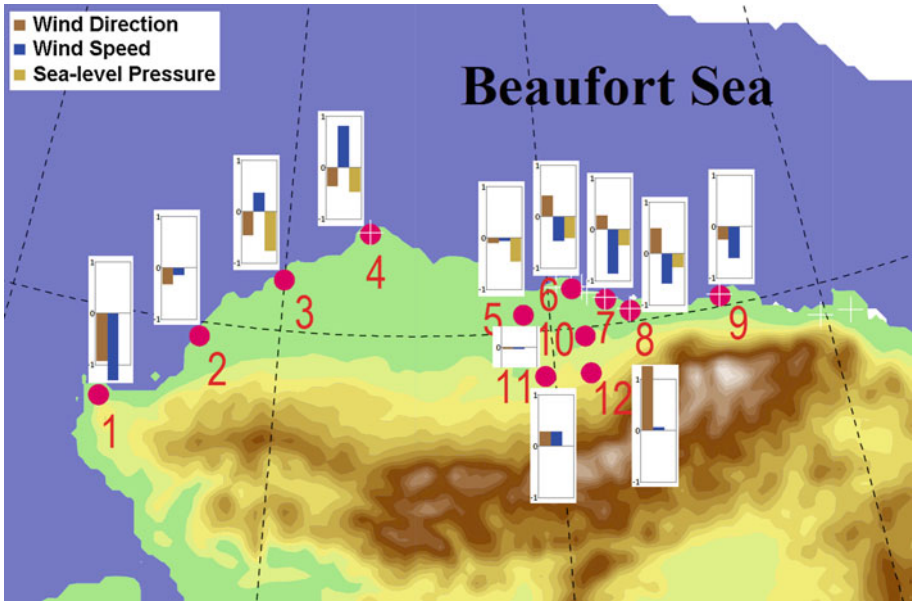


**Fig. 8** Difference in root-mean-square errors for experiments QSCAT and CTRL (QSCAT–CTRL) of 10-m wind speed (m $s^{-1}$), wind direction (40°), and sea-level pressure (hPa) at model simulation hour 18, averaged over all eight cases, for each of the 12 individual stations. See Fig. 1 for station identification

west for stations Nos. 1 through 5, and again in the east at station No. 9. The degradation in the wind-direction forecast in the middle of the northern coast is likely associated with the model background error pattern as discussed in Sect. 4.1. Wind speed was improved at most coastal stations except for Nos. 3 and 4. Insignificant improvement was seen at the slightly inland station No. 10 and forecasts were degraded at the two far-inland stations Nos. 11 and 12.

Part of the inconsistency between the verification results when using QuikSCAT versus station data is most likely due to the difficulty in accurately interpolating from a 10-km grid over a region with variable topography and/or variability associated with the coastal environment. Over the open ocean, these issues are less applicable, and the interpolated forecast is therefore more representative of the skill of the model. Thus, it is very encouraging to see the consistent improvements in the forecasting of surface winds when verified against QuikSCAT data, which suggests that the analyses are being reliably improved through their assimilation, at least as far as winds are concerned.

### 4.3 Impacts on the Atmospheric Boundary Layer and Low-Level Atmosphere

The previous sections focused on discussions of the impacts of assimilating QuikSCAT data on the surface variables in the 3D-VAR analysis and the WRF forecasts. In this section, we focus on the impacts on the atmospheric boundary layer and low-level atmosphere and investigate how the impact of the assimilation of ocean near-surface winds propagates through the boundary layer and into the free atmosphere. The analysis first focuses on a discussion of the differences between the two experiments, followed by their validation with independent observations from soundings, wind profilers, as well as the NARR re-analysis.

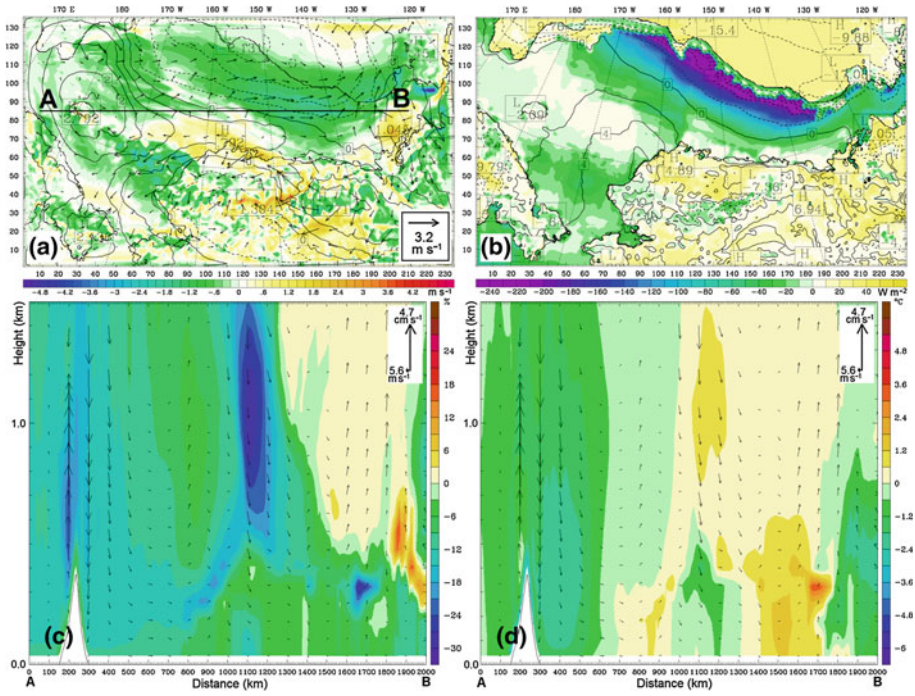


**Fig. 9** Difference fields between the QSCAT and CTRL experiments (QSCAT–CTRL) for: **a** surface wind speed at 10-m height (m $s^{-1}$, *shaded*) and vectors and sea-level pressure (hPa, *contour*); **b** total upward (sensible + latent) heat flux at the surface (W $m^{-2}$, *shaded*); **c** relative humidity (%, *shaded*) and circulation vectors along cross-section AB as shown in (**a**); and **d** air temperature (°C, *shaded*) and circulation vectors along cross-section AB. All fields are valid at 0600 UTC 1 Oct 2002. *Contours* in (**b**) are actual surface air temperature (°C) from the QSCAT experiment

### *4.3.1 Comparisons Between Experiments*

Figure 9 shows, as an example, a comparison of the QSCAT and CTRL experiments at 0600 UTC 1 October 2002. This case was initialized at 0000 UTC and data were assimilated three times at 0200, 0400, and 0600 UTC (ref. Fig. 3). Figure 9a shows that the wind speed in the QSCAT experiment was reduced over most of the open water areas compared to CTRL, except for the south-western and south-eastern Beaufort Sea off the coasts of Alaska and the Northwest Territories, respectively. Sea-level pressure increased markedly over the Chukchi Sea, while a smaller increase is seen over the eastern Brooks Range and a large decrease is found over the central Beaufort Sea. As expected, anticyclonic differences in wind direction accompany the increases in sea-level pressure while cyclonic differences in direction correspond to areas of pressure decrease, as indicated by the wind-vector differences. In other words, the assimilation of ocean surface winds had a direct impact on the wind field. At the same time, the sea-level pressure field was also affected in a dynamically consistent manner through mass adjustment.

The contour lines in Fig. 9b show the surface air temperature field from the QSCAT experiment. The zero contour line is parallel to the ice edge in the middle of the Beaufort Sea, though the water remained warmer than the air throughout nearly the entire domain (not shown). The shaded colours in Fig. 9b show the differences in total upward heat flux

(sensible + latent) at the surface between the two experiments. Upward heat flux is reduced over nearly all areas of open water, and is associated primarily with areas of decreased wind speeds (see Fig. 9a) in the QSCAT experiment. These lessened wind speeds lead to reduced latent heat (through reduced evaporation) and sensible heat transfer to the atmosphere from the underlying warmer ocean water.

Such changes in surface heat fluxes can have a significant impact on low-level temperature and humidity through the reduction of available heat and moisture to the boundary layer. To illustrate this, changes in the vertical dimension between the two experiments are given in Fig. 9c, d, which show the differences in relative humidity and air temperature, respectively, along with vertical circulation vectors along the cross-section AB (see Fig. 9a). Lower-level relative humidity was decreased in the QSCAT run along the entire cross-section; on the eastern side, however, this change was contained within the boundary layer, which extended to roughly 500 m in height. This difference in the east is associated with the increase in wind speed seen at the eastern end of line AB in Fig. 9a, which resulted in greater evaporation and thus increased available moisture there compared to points farther west in the cross-section.

The air temperature within the boundary layer is related to the vertical circulations (Fig. 9d), as well as to changes in surface wind speed (ref. Fig. 9a). The differences in vertical circulation between experiments QSCAT and CTRL show an area of stronger sinking motion on the western end of line AB, an area of less stronger sinking motion in the middle section, and an area of weak sinking motion on the eastern end in QSCAT. All three areas are associated with surface anticyclonic differences in wind direction (see Fig. 9a), and are also areas of high sea-level pressure differences. These three-dimensional flow patterns in the difference field caused mixing of cold upper air with surface air and resulted in the reduced air temperature seen in Fig. 9d. The area of large reduction in surface wind speed in the central Beaufort Sea off the Alaskan coast, together with the weak vertical mixing, led to the increased air temperature in the QSCAT experiment in the eastern half of the cross-section (Fig. 9d). In subsequent hours, the impact from the data assimilation period weakened, and after six hours of free forecast, the boundary-layer structure was again stabilized and well defined and, therefore, smaller differences between the two experiments were observed at 1200 UTC (not shown).

#### *4.3.2 Validation with Observations and Re-Analysis*

To further investigate the impacts of data assimilation on the boundary layer and model forecasts, simulations from both experiments QSCAT and CTRL were compared with radiosonde observations from Barrow, Alaska (red dot location 4 in Fig. 1) and radar wind-profiler data from the Atmospheric Radiation Measurement program (http://www.arm.gov), also located in Barrow. Hourly radar wind-profiler data were only available for one day in the study period: 1 October 2002. Modelled wind profiles showed good agreement with the profiler winds for the prevailing wind patterns (not shown).

For each of the eight modelled cases, radiosonde observations at Barrow were also used for verification. The available 1200 UTC and 0000 UTC observation times correspond to model simulation hours 12 and 24 (free-forecast hours 6 and 18), respectively. The radiosonde data are available at 12 pressure levels as shown in Table 2; the model data were interpolated onto these levels for verification. Table 2 shows the differences in absolute errors for temperature and *U*- (zonal) and *V*- (meridional) winds between the QSCAT and CTRL experiments (QSCAT–CTRL). Negative values signify that the QSCAT forecasts have smaller absolute errors than CTRL. From this single-station comparison, we see that the impacts from the assimilation of ocean near-surface winds can propagate throughout the entire model

**Table 2** Difference in root-mean-square errors between the QSCAT and CTRL experiments (QSCAT–CTRL) for model temperature and *U*- and *V*-wind components against radiosonde observations at Barrow, Alaska

| Pressure levels (hPa) | 2002 | | | | | | 2004 | | | | | |
|---|---|---|---|---|---|---|---|---|---|---|---|---|
| | Temperature (°C) | | *U*-wind (m s$^{-1}$) | | *V*-wind (m s$^{-1}$) | | Temperature (°C) | | *U*-wind (m s$^{-1}$) | | *V*-wind (m s$^{-1}$) | |
| | 1200 (6 h) | 0000 (18 h) | 1200 (6 h) | 0000 (18 h) | 1200 (6h) | 0000 (18 h) | 1200 (6 h) | 0000 (18 h) | 1200 (6 h) | 0000 (18 h) | 1200 (6 h) | 0000 (18 h) |
| 50 | 0.03 | **−0.27** | 0.23 | 0.19 | **−0.24** | 0.04 | 0.42 | 0.11 | 0.34 | **−0.08** | 0.57 | 0.23 |
| 100 | **−0.06** | **−0.07** | 0.42 | **−0.28** | 0.01 | **−0.06** | 0.03 | **−0.09** | 0.11 | **−0.15** | 0.74 | 0.35 |
| 150 | **−0.14** | **−0.05** | 0.01 | **−0.01** | 0.05 | 0.00 | 0.14 | 0.09 | **−0.11** | **−0.17** | **−0.07** | 0.04 |
| 200 | **−0.08** | 0.09 | 0.03 | **−0.21** | **−0.24** | 0.17 | 0.05 | **−0.07** | 0.29 | **−0.18** | 0.36 | 0.11 |
| 250 | 0.08 | 0.12 | **−0.20** | 0.13 | 0.17 | **−0.12** | **−0.09** | 0.01 | 0.33 | 0.32 | 0.63 | 0.09 |
| 300 | **−0.09** | 0.00 | **−0.17** | 0.13 | 0.29 | 0.01 | 0.13 | 0.27 | 0.09 | 0.05 | 0.35 | **−0.55** |
| 400 | 0.10 | 0.01 | **−0.17** | 0.16 | 0.04 | 0.00 | **−0.22** | 0.12 | **−0.91** | **−0.64** | **−0.36** | **−0.23** |
| 500 | **−0.01** | **−0.01** | **−0.16** | **−0.02** | **−0.32** | 0.15 | 0.10 | 0.04 | 0.10 | **−0.22** | **−0.55** | 0.53 |
| 700 | **−0.22** | 0.16 | 0.33 | 0.14 | **−0.18** | **−0.36** | **−0.12** | 0.07 | **−0.29** | 0.07 | **−0.08** | **−0.30** |
| 850 | **−0.37** | 0.09 | 0.30 | 0.38 | 0.05 | 0.21 | 0.27 | 0.32 | 0.27 | **−0.68** | **−0.31** | 0.30 |
| 925 | 0.01 | 0.09 | 0.45 | 0.55 | 0.46 | 0.38 | 0.27 | **−0.10** | **−1.72** | **−0.92** | **−0.13** | 0.56 |
| 1,000 | 0.05 | **−1.01** | 0.22 | 1.45 | 0.88 | 0.25 | | | | | | |

For each of the eight cases, 1200 UTC and 0000 UTC correspond to 6-h and 18-h free forecast (6-h assimilation period ended at 0600 UTC). Negative values are shown in bold

atmosphere. In the 2002 cases, greater improvement is seen in the upper-air temperature field, whilst the 2004 cases show more direct improvement in the lower-level winds.

A relative lack of conventional observations over the remote, high-latitude regions both limits the information available for data assimilation and makes model verification difficult, particularly above the surface. Lacking additional observations for upper-air verification, we therefore turn to the NARR re-analysis as another source of information to validate the model simulations in order to investigate how assimilation affects the boundary layer and lower atmosphere throughout the entire model domain.

NARR data are available at an interval of three hours. At each model output time for which NARR data are available, the root-mean-square error relative to NARR was calculated over the entire model domain for planetary boundary-layer height and surface upward sensible and latent heat fluxes. Figure 10a shows the difference in the root-mean-square error between the QSCAT and CTRL runs for these three variables at three-hourly intervals of the model simulation. Negative values signify that the QSCAT experiment produced smaller errors than CTRL. The heavy solid lines show the average for each variable over all eight cases. We see that the two experiments commenced from the same initial state. During the assimilation period, all three variables exhibit large differences in error, indicating that the model states are undergoing a period of adjustment. While the error in planetary boundary-layer height was larger in the QSCAT run than in CTRL during the assimilation period, the error was greatly reduced immediately after assimilation and gradually improved relative to the CTRL experiment during the free-forecast period. The upward sensible and latent heat fluxes in the QSCAT run had much smaller errors than in CTRL during the assimilation period. This suggests that the QuikSCAT winds were consistently directly improving heat fluxes as they were assimilated. After the assimilation period, QSCAT heat fluxes were still more realistic than in CTRL, though the improvement was no longer as pronounced as during assimilation.

At 850 hPa, the root-mean-square error was calculated for geopotential height, temperature, relative humidity, and $U$- and $V$-wind components. Figure 10b shows the differences in root-mean-square error between the QSCAT and CTRL experiments, where negative values indicate smaller errors in QSCAT. The adjustment period occurring during data assimilation can also be seen here for all the variables shown. After the assimilation period, all five variables in the QSCAT experiment began to improve. The most pronounced of these is the $U$-wind component. The error in the QSCAT run increased relative to CTRL as soon as QuikSCAT data were introduced. However, after a 3-h adjustment, the $U$-wind component was greatly improved upon the subsequent assimilation of additional QuikSCAT data. By the end of the assimilation period, the $U$-wind component in the QSCAT run had already significantly improved over CTRL, an improvement that was maintained throughout the entire free-forecast period. The $V$-wind component exhibited a more gradual improvement after the initial adjustment period, and showed reduced error in the QSCAT run after 12 hours of free forecast. The less-significant improvement in the meridional wind is most likely due to the prevailing winds in the region being zonal; both the model background and QuikSCAT meridional winds were weak. Among the variables investigated, geopotential height exhibited the weakest impact from data assimilation. Nevertheless, it also gradually improved throughout the course of the QSCAT run, and after 12 h of free forecast was better in QSCAT than in CTRL. There were adverse effects on the 850-hPa temperature and relative humidity from the assimilation of ocean surface winds. However, in a similar fashion to the QSCAT wind field and circulation that began their adjustment toward an improvement immediately after assimilation, the negative effects seen in temperature and relative humidity caused by assimilation were gradually reduced during the free-forecast period.

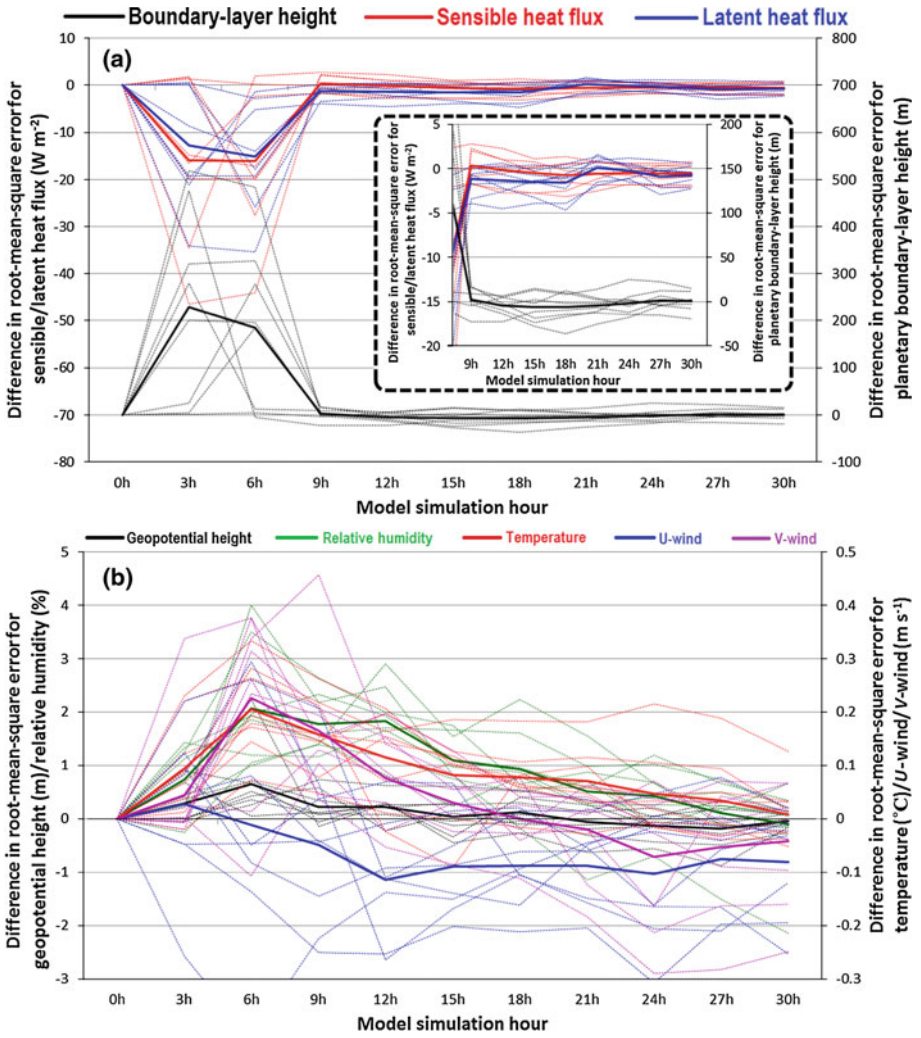


**Fig. 10** Difference in root-mean-square error between the QSCAT and CTRL experiments (QSCAT–CTRL) for: **a** planetary boundary-layer height (m) and surface upward sensible and latent heat fluxes (W $m^{-2}$); **b** 850-hPa level geopotential height (m), relative humidity (%), temperature (°C), and *U*- and *V*-wind components (m $s^{-1}$). For each variable, the *thin dotted lines* represent each individual case and the *heavy solid line* is their average. The *insert* in (**a**) is an amplified portion of the free-forecast period

## 5 Summary

This study demonstrated the successful assimilation of QuikSCAT ocean near-surface wind speed and direction data into the WRF model via the 3D-VAR assimilation approach, utilizing customized WRF model background error and QuikSCAT observational error calculated from an observational analysis. Through a modelling study of eight cases and verification of model forecasts against QuikSCAT data, station observations, as well as the NARR re-analysis, the following conclusions were reached:

- Impacts on the 3D-VAR analysis of wind fields are consistent with the QuikSCAT observations, implying the robustness and success of the assimilation approach.
- Verification with unassimilated QuikSCAT observations during free-forecast periods shows significant improvements for surface wind forecasts, which also demonstrates the temporal consistency and quality of QuikSCAT observations.
- Verification with coastal land-station observations shows significant and consistent improvement in sea-level pressure, reducing both root-mean-square error and bias. The wind fields, after the assimilation and model adjustment period, showed reduced error and bias. Verification at individual stations showed consistent improvement for sea-level pressure. Winds at farther inland stations had reduced impacts. Errors in wind speed along the northern coast of Alaska and wind direction in the western region were reduced.
- The assimilation of QuikSCAT data demonstrates physically and dynamically consistent impacts between the surface and upper air. Domain-wide improvement in the surface wind field, planetary boundary-layer height, and sensible and latent heat fluxes propagated upward into the lower atmosphere. 850-hPa wind and geopotential height were improved during free-forecast periods.

The above modelling results suggest that QuikSCAT winds are a potentially highly valuable resource for the simulation of ocean surface winds, and certainly merit further study for assimilation into numerical models.

**Acknowledgments** This work was supported by funding from the Bureau of Ocean Energy Management of the U.S. Department of the Interior under contract 0106CT39787 and by funding from the National Oceanic and Atmospheric Administration (NOAA) under project SOVACC. Computational support was provided by the Arctic Region Supercomputing Center (ARSC) at the University of Alaska Fairbanks (UAF).

## References

Barker DM, Huang W, Guo YR, Xiao QN (2004) A three-dimensional (3DVAR) data assimilation system for use with MM5: implementation and initial results. Mon Weather Rev 132:897–914

Bengtsson L, Ghil M, Kallen E (1981) Dynamic meteorology: data assimilation methods. Springer, New York, 330 pp

Chen SH (2007) The impact of assimilating SSM/I and QuikSCAT satellite winds on Hurricane Isidore simulations. Mon Weather Rev 135:549–566. doi:10.1175/MWR3283.1

Chen F, Dudhia J (2001) Coupling an advanced land-surface/hydrology model with the Penn State/NCAR MM5 modelling system. Part I: Model description and implementation. Mon Weather Rev 129:569–585

Chen SH, Vandenberghe F, Petty GW, Bresch JF (2004) Application of SSM/I satellite data to a hurricane simulation. Q J R Meteorol Soc 130:801–825

Daley R (1991) Atmospheric data analysis. Cambridge University Press, New York, 457 pp

Dudhia J (1989) Numerical study of convection observed during the winter monsoon experiment using a mesoscale two-dimensional model. J Atmos Sci 46:3077–3107

Hong SY, Dudhia J, Chen SH (2004) A revised approach to ice microphysical processes for the bulk parameterization of clouds and precipitation. Mon Weather Rev 132:103–120

Ide K, Courtier P, Ghil M, Lorenc A (1997) Unified notation for data assimilation: operational, sequential and variational. J Meteorol Soc Jpn Special Issue 75(1B):181–189

Isaksen L, Janssen PAEM (2004) Impact of ERS scatterometer winds in ECMWF's assimilation system. Q J R Meteorol Soc 130:1793–1814

Janjic ZI (1990) The step-mountain coordinate: physical package. Mon Weather Rev 118:1429–1443

Janjic ZI (1996) The surface layer in the NCEP eta model. In: Eleventh conference on numerical weather prediction, Norfolk, VA, 19–23 August, American Meteorological Society, Boston, pp 354–355

Janjic ZI (2002) Nonsingular implementation of the Mellor-Yamada level 2.5 scheme in the NCEP meso model. NCEP Office Note, No. 437, 61 pp

Kain JS, Fritsch JM (1990) A one-dimensional entraining/detraining plume model and its application in convective parameterization. J Atmos Sci 47:2784–2802

Kain JS, Fritsch JM (1993) Convective parameterization for mesoscale models: the Kain-Fritcsh scheme. In: Emanuel KA, Raymond DJ (eds) The representation of cumulus convection in numerical models. American Meteorological Society, Boston, 246 pp

Kalnay E (2003) Atmospheric modelling, data assimilation and predictability. Cambridge University Press, New York, 341 pp

Kistler R, Kalnay E, Collins W, Saha S, White G, Woollen J, Chelliah M, Ebisuzaki W, Kanamitsu M, Kousky V, van den Dool H, Jenne R, Fiorino M (2001) The NCEP-NCAR 50-year reanalysis: monthly means CD-ROM and documentation. Bull Am Meteorol Soc 82:247–267. doi:10.1175/1520-0477(2001)082<0247:TNNYRM>2.3.CO;2

Kozo T (1980) Mountain barrier baroclinity effects on surface winds along the Alaskan coast. Geophys Res Lett 7:377–380

Kozo T (1982) An observational study of sea breezes along the Alaskan Beaufort Sea coast: part I. J Appl Meteorol 21(7):891–905

Leidner SM, Isaksen L, Hoffman RN (2003) Impact of NSCAT winds on tropical cyclones in the ECMWF 4DVAR assimilation system. Mon Weather Rev 131:3–26

Long DG, Mendel JM (1990) Model-based estimation of wind fields over the ocean from wind scatterometer measurements. I. Development of the wind field model. IEEE Trans Geosci Remote Sens 28(3):349–360

Mesinger F, DiMego G, Kalnay E, Mitchell K, Shafran PC, Ebisuzaki W, Jović D, Woollen J, Rogers E, Berbery EH, Ek MB, Fan Y, Grumbine R, Higgins W, Li H, Lin Y, Manikin G, Parrish D, Shi W (2006) North American regional reanalysis. Bull Am Meteorol Soc 87:343–360. doi:10.1175/BAMS-87-3-343

Mlawer EJ, Taubman SJ, Brown PD, Iacono MJ, Clough SA (1997) Radiative transfer for inhomogeneous atmosphere: RRTM, a validated correlated-k model for the long wave. J Geophys Res 102(D14):16663–16682

Parrish DF, Derber J (1992) The National Meteorological Center's spectral statistical interpolation analysis system. Mon Weather Rev 120:1747–1763

Pichel W, Monaldo F, Nicoll J (2005) SAR-derived coastal winds. Alaska Satellite Facility News and Notes, winter 2:4

Skamarock WC, Klemp JB, Dudhia J, Gill DO, Barker DM, Wang W, Powers JG (2005) A description of the advanced research WRF version2. NCAR Technical Note, NCAR/TN-468+STR, 88 pp

Stegall ST, Zhang J (2012) Wind field climatology, changes, and extremes in the Chukchi–Beaufort Seas and Alaska North Slope during 1979–2009. J Clim 25:8075–8089. doi:10.1175/JCLI-D-11-00532.1

Talagrand O (1997) Assimilation of observations, an introduction. J Meteorol Soc Jpn Special Issue 75(1B):191–209

Thompson DW, Wallace JM (1998) The Arctic Oscillation signature in the winter time geopotential height and temperature fields. Geophys Res Lett 25:1297–1300

Walsh JE, Chapman WL, Shy TL (1996) Recent decrease of sea level pressure in the central Arctic. J Clim 9:480–488

Zhang X, Walsh JE, Zhang J, Bhatt US, Ikeda M (2004) Climatology and interannual variability of Arctic cyclone activity: 1948–2002. J Clim 17:2300–2317